Carbohydrate Polymers 235 (2020) 115866

Contents lists available at ScienceDirect

Carbohydrate Polymers

journal homepage: www.elsevier.com/locate/carbpol

Structure and properties of helical fibers spun from cellulose solutions in $[B_{mim}]Cl$☆

Sergey V. Usachev[a], Dmitry V. Zlenko[a,b,*], Irina V. Nagornova[c], Elena V. Koverzanova[a], Mariya G. Mikhaleva[a], Alexander S. Vedenkin[a], Daria N. Vtyurina[a], Aleksey A. Skoblin[a], Sergey N. Nikolsky[a], Galina G. Politenkova[a], Sergey V. Stovbun[a]

[a] N.N. Semenov Institute of Chemical Physics RAS, Moscow, Russia
[b] M.V. Lomonosov Moscow State University, Moscow, Russia
[c] Moscow Polytechnic University, Moscow, Russia

ARTICLE INFO

Keywords:
Cellulose
Ionic liquid
Chirality
Fiber

ABSTRACT

Man-made fibers were spun from solutions of cotton and wood cellulose in ionic liquid (1-butyl-3-methyl-imidazolium chloride, $[B_{mim}]Cl$). Depending on the concentration, cellulose dissolved in $[B_{mim}]Cl$ down to macromolecules or nanofibrils. The artificial fibers had a diameter of about 100 nm, were uniform, transparent, helical, and optically active. The fibers were composed of the core and shell (~20% of the radius). The core was composed of the dense helical pseudofibrils of about 30 nm in thick occupying of about 40% of the area of the fiber core cross-section. The tensile strength of the whole fiber was, on average, 250 MPa, while that of the individual pseudofibrils was ~1.1 GPa. The tensile-strength dependencies were two-stage with drastically different Young's modules. We explain the shape of the loading curves as well as the strength of the fibers by the friction between the twisted pseudofibrils in the core.

1. Introduction

Cellulose is a widespread and biodegradable polymer, which makes it a perspective raw for the modern "green" industry, including the high-strength fibers production (Lundahl, Klar, Wang, Ago, & Rojas, 2017; Oksman et al., 2016). The advantages of the cellulose as a raw material justifies the cost of the production of the fibers (Lundahl et al., 2017). On the other hand, the relations of the fibers' properties with the origin of the cellulose raw and pretreatment techniques are poorly explained, as the universal model of the cellulose structure and packing in man-made fibers and films has not been developed yet. Some authors emphasize that the available data on the cellulose structure cannot explain the effects observed in the cellulose solutions (Lundahl et al., 2017). The generalized description of the cellulose structure is additionally hindered by structural diversity of cellulose varying in dependence on its origin (Hult, Larsson, & Iversen, 2001; Jarvis, 2003; Newman, 1999; Zhao & Li, 2014).

Cotton and linen cellulose is the most popular raw for the fibers' production due to the length of the natural fibers which is sufficiently large for spinning. Wood cellulose is cheaper but could not be directly used for fibers' spinning as the wood fibers are shorter. This problem was solved by the viscose process that allowed producing of synthetic cellulose fibers since the late XIX century (Cross & Bevan, 1892). The widespread of this technology significantly broadened the assortment of textile fabrication. However, it is characterized by some disadvantages primarily related to environmental pollution (Vanhoorne et al., 1991).

The cellulose dissolves in various mixtures based on the organic solvents and inorganic salts (Dawsey & McCormic, 1990; Heinze & Koschella, 2005; Kostag, Jedvert, Achtel, Heinze, & Seoud, 2018; Perepelkin, 2007). Despite the effectiveness of the cellulose dissolution, most of these solvents failed to become widespread in the industry due to the complexities of their regeneration. Therefore, the development of the cellulose mono-solvents is of particular interest, as they could be regenerated and recycled easily. In 1934, Graenacher reported the technique of effective cellulose dissolving by benzylpyridinium chloride (Graenacher, 1934). However, due to the high melting temperature (118°), the industrial application of this solvent was limited. Later, some tertiary amine-oxides were shown to be effective cellulose solvents (Graenacher & Sallmann, 1939), and the best one was N-methylmorpholine N-oxide (NMMO). NMMO is used as the cellulose

☆ The work was supported by FASO Russia, theme number 45.9, 0082-2014-0011, AAAA-17-117111600093-8.
* Corresponding author at: M.V. Lomonosov Moscow State University, Moscow, Russia.
E-mail address: dvzlenko@gmail.com (D.V. Zlenko).

https://doi.org/10.1016/j.carbpol.2020.115866
Received 13 September 2019; Received in revised form 27 December 2019; Accepted 12 January 2020
Available online 23 January 2020
0144-8617/

solvent in the Liocell® process of man-made fibers production. The cellulose solution is precipitated by water, and NMMO can be then separated and fully recycled (Perepelkin, 2007).

For the first time, ionic liquids (salts of organic solvents with the low melting temperature, IL) were used for cellulose dissolution in 2002 (Swatloski, Spear, Holbrey, & Rogers, 2002). Variating of both the anions and structure of the imidazoline cation allowed creating ILs melting at room temperature (Fukaya, Sugimoto, & Ohno, 2006). Some of IL dissolve cellulose well and do not cause its destruction (Kostag et al., 2018). The best results were obtained using the ionic liquids based on dialkyl-imidazoline combined with different anions (Swatloski et al., 2002). Moreover, ILs allow obtaining the molecular solutions of cellulose as it was demonstrated for the N-ethyl-N-methylimidazolyl acetate (Song, Niu, Wang, & Zhang, 2011). ILs are single-component solvents, which allows extracting them from the aqueous solution after cellulose precipitating and returning into the technological process (Asaadi et al., 2016; Hina, Zhang, & Wang, 2015).

The fibers' production process is composed of two main stages: the dissolution of cellulose and the drawing-out of the fibers followed by precipitation in water. The cellulose dissolving is a quite complicated process that starts with the swelling stage and can finish by full cellulose dissolution (Endo, Hosomi, Fujii, Ninomiya, & Takahashi, 2016; Song et al., 2011; Zhang, Cui, Lynd, & Kuang, 2006). Herein, the process of cellulose dissolution cannot be considered out of touch with the hierarchical structure of cellulose composed of several structural levels (Nikolsky, Zlenko, Melnikov, & Stovbun, 2019; Raabe, Sachs, & Romano, 2005). In the native cellulose, the chains are combined into the helical elementary fibrils (nanofibrils) having a diameter of 2.5 nm in wood, and up to 20 nm in cellulose from tunicates (Hult et al., 2001; Jarvis, 2003; Newman, 1999; Zhao & Li, 2014). The nanofibrils in their turn form helical microfibrils having a diameter of 20–40 nm(Hanley, Giasson, Revol, & Gray, 1992; Hanley, Revol, Godbout, & Gray, 1997).

In case if the cellulose macromolecules do not degrade, the dissolution of super-helical fibrils can proceed only through their sequential untwisting since other ways of chains' dissociation are limited by the friction force (Nikolsky et al., 2019). Due to the rather high weight of the cellulose chains and nanofibrils, the untwisting process typically takes hours. Therefore, the mutual orientation of the chains seems not to become chaotic in the course of the dissolution. Accordingly, the cellulose "solutions" often retain noticeable structural ordering despite the visual homogeneity (Boerstoel, Maatman, Westerink, & Koenders, 2001; Morgenstern & Kammer, 1999; Zhang et al., 2006). Local ordering in solutions of cellulose can be useful in fibers' spinning process, as the tangential loads in a spinneret can magnify the spatial scale of the anisotropy. Such an effect was demonstrated by X-ray diffractometry for the hardwood cellulose (Lundahl et al., 2017). Moreover, the core of the man-made cellulose fiber forms as the result of the ordering and association of the crystalline nanofibrils (Lundahl et al., 2017).

The methodology of the spinning defines the basic properties of the fibers. The spinneret nozzle diameter, the extrusion rate, the elongation ratio, and coagulation basin temperature affect the fibers' strength (Kim, Pak, Jo, & Lee, 2005; Lundahl et al., 2017; Michud, Hummel, & Sixta, 2016). It is generally accepted that the strength of the cellulose crystallite is provided by hydrogen bonding between the cellulose chains (Meyer & Misch, 1937). However, the theoretical studies show that Young's modulus of the cellulose chain is provided by the intramolecular hydrogen bonds between the hydroxyl groups of the 2nd and 6th atoms of the neighboring residues (Tashiro & Kobayashi, 1990). The same result was obtained in the experiments on the stretching of the swollen cellulose films (Hishikawa, Togawa, & Kondo, 2010).

Cold alkaline treatment (mercerization) is usually used to increase the amount of α-cellulose in wooden raw (Kamide, Okajima, & Kowsaka, 1992; Richter, 1929). Mercerization is accompanied by the reorganization of the cellulose chains' packing known as the formation of cellulose-II (Dinand, Vignon, Chanzy, & Heux, 2002; Langan, Nishiyama, & Chanzy, 1999). The cellulose-II monocrystals have lower Young's modulus (88 GPa) compared to the initial cellulose-I (138 GPa) as it was shown for the cellulose of various origin (Nishino, Takano, & Nakamae, 1995). This result explains the lower strength of the fibers made of the cellulose mercerized by more than 2% alkaline solution (Oudiani, Chaabouni, Msahli, & Sakli, 2011).

The quality of the final man-made fiber depends on average length of the cellulose chains. Using of the cellulose with higher degree of polymerisation (DP) and, respectively, longer initial chains provides for the better ordering inside the fibers at the production stage (Lundahl et al., 2017) which results in the improvement of the mechanical properties (Kim et al., 2005). On the other hand, DP of 500–800 is considered to be optimal for Liocell® process (Rabideau & Ismail, 2015; Sealey, Persinger, Luo, Roscelli, & Neogi, 2002). For the cellulose solutions in IL containing N-alkylimidazoline cation, the spinning was shown to be efficient at DP within the range 514–920 for the raw of different origin, and up to 1180 in case of beech cellulose (Hummel et al., 2006).

The fibers could also be fabricated of the nanocellulose dispersions rather than its solutions. The hydrodynamic compression technique allowed orienting of the cellulose nanofibrils (CNF) in parallel to each other, which resulted in the fibers of a very high tensile strength equal to 1.2 GPa (Mittal et al., 2018). The 1,2,3,4-butane-tetracarboxylic acid treatment led to the fibers with the strength of 1.6 GPa (Mittal et al., 2018). The fibers characterized by a similar tensile strength (1.7 GPa) were fabricated by extrusion into the phosphoric acid solution (Northolt et al., 2001). At the same time, the fibers produced by spinning from the cellulose solutions in the ionic liquids had tensile strength values of about 0.5 GPa (Hummel et al., 2006).

In this study, we discuss both the dissolution of cellulose in $[B_{mim}]Cl$ and the spinning of the fibers using the obtained solutions. We have used the mercerized and unmercerized celluloses from wood and cotton as the initial raw. The resulting fibers had a distinct helical structure, were consisted of numerous thin (~20 nm) pseudo-fibrils and had the overall diameter of about 100 μm. Both, the strength and elasticity of the prepared fibers allow recommending them for ballistic fabrics manufacturing.

2. Materials and methods

In this work, we compared two sources of cellulose: the lignin-free and expansive cotton cellulose and the cellulose from hardwood that initially contains a lot of lignin, but cheaper. Cotton cellulose was both from fibers and lint to verify the influence of the initial degree of polymerization. The cellulose was obtained from two different sources: bleached kraft soft-wood cellulose (Arkhangelsk paper and pulp mill, Russia), cotton linter, and cotton fiber (UzCell, Uzbekistan). Before use, the hardwood and cotton linter cellulose were mercerized using 17.5% solution of caustic soda (room temperature, 30 min, 15 kg/kg) to increase the α-cellulose content (Richter, 1929) and improve the solvation. The mercerized pulp was drained with a distilled water on the glass filter until the neutral pH and then dried at 80–90°. The α-cellulose content was measured according to the standard methodology (GOST 6840-78). The degree of polymerization of cellulose was determined according to the viscosity of copper-ammonium solution (Whorlow, 1980).

The hardwood cellulose was characterized by the initial DP of 1800–1850, which decreased to 1400–1450 after mercerization. The DP of initial cotton linter before and after mercerization was lower than for the hardwood cellulose (1400–1650, and 1250–1500, correspondingly). The exact DP of the cotton fiber cellulose was not determined due to very high viscosity of copper-ammonium solution, but we can state it was greater than 10,000. The α-cellulose content in wood cellulose before mercerization was 84 ± 3% and increased to 97 ± 1% after alkaline treatment. In cotton cellulose, the initial fraction of α-cellulose was much higher and reached 96 ± 3%. Ash content in mercerized

wood cellulose (0.11 ± 0.02%) was lower than in cotton linter and fibers (0.20 ± 0.03%). All of the further experiments were made using mercerized hardwood and cotton linter cellulose, and untreated cotton fiber cellulose.

The ionic liquid (1-butyl-3-methyl-imidazolium chloride, $[B_{mim}]Cl$) was synthesized in reaction of 3-methyl-imidazolium with a 1-butyl chloride in acetonitrile (molar ratio of the components was 1:1.2:3). The reaction was held in the closed vessel at 100 °C for 8 h (usually the process is held at 80 °C for 48 h (Dupont, Consorti, Suarez, & de Souza, 2003). The solvent and unreacted components were removed by the rotary vacuum evaporator. The residual was a viscous yellowish liquid (Fendt, Padmanabhan, Blanch, & Prausnitz, 2011; Sescousse, Le, Ries, & Budtova, 2010). The yield of the $[B_{mim}]Cl$ was 98.3%, and the purity 98.5% according to ^1H NMR (D_2O, 500.18 Hz); δ: 0.95 (t, 3H, $CH_2 - \underline{CH_3}$), 1.27 (m, 2H, $\underline{CH_2}$-CH_3), 1.35 (m, 2H, CH_2), 3.92 (s, 3H, N-CH_3), 4.22 (m, 2H, N-CH_2), 7.46 and 7.50 (1H & 1H, CH = CH *Im*), 8.73 (1H, N-C(H)-N *Im*). The NMR spectra were registered using Avance III 500 spectrometer (Bruker, Germany).

The dissolution of cellulose in $[B_{mim}]Cl$ was held in an oil bath at two temperatures. In the first case, the temperature was set to 105 ± 2 °C, and the dissolution required 3 h (stirring 80–90 rpm). The residual gas bubbles were removed under vacuum (5 Torr). In the second case, we tried to dissolve the cellulose at 130 ± 2 °C, which took only 1.0–1.5 h, and no gas bubbles were forming. But, the cellulose solutions obtained at 130 °C become a little bit stained. Therefore, all the further experiments were carried out using the cellulose dissolved at 105 °C.

The solubility limit of 7% was obtained for mercerized hardwood and cotton linter cellulose. In contrast, the upper limit of dissolution for the cellulose from the cotton fiber was found to be about 4%. Moreover, the cotton fiber cellulose never fully dissolved, which significantly complicated the experiments. Above these thresholds, the viscosity of the solutions became so high that their degasification and extrusion became impossible. For fibers producing, we used the solutions of 5% and 3% for hardwood/linter, and fiber cellulose, respectively.

The structure of cellulose solutions was investigated using synchrotron radiation diffraction technique: 1.445 Å, Pilatus3 1M detector (Dectris, Switzerland) at NIC Kurchatovsky Institute (Moscow, Russia).

Films were prepared by coagulation of the cellulose solutions of a rather low concentration (0.1–1.0%). The contiguous and strong films were made as follows: a glass rod with a glass ball at the end was immersed in the cellulose solution, and then to water. As a result, a thin cellulose film formed on the glass ball's surface.

The fibers were produced by the cellulose solution extruding through a spinneret with the rate of 8–12 cm/s (Fig. 1). The resulting thin thread of solution fell freely into a bath filled with cold distilled water. The diameter of the spinneret was 125 μm, the length of the spinneret channel was 15 mm. The additional experiments were carried out with a spinneret elongated up to 70 mm. The temperature of the cellulose solution in the course of the extrusion was maintained at 70 or 90 °C. The distance from the edge of the spinneret to the surface of the water in the precipitation bath was 15 cm. The additional experiments were carried out with the distance to the water surface increased to one meter or decreased to zero. After the precipitation, the obtained fibers were wounded on spools and washed in distilled water for 24 h. Drying of the fibers was carried at 23 ± 2 °C and ambient humidity of 40–45%. The length of a fiber obtained in a single extrusion act was 40–50 cm.

MIKMED-6 optical microscope was used for fibers' overall structure and homogeneity analysis. The electron microscopy analysis was made using a JSM 7500F scanning electron microscope (JEOL, Japan). The spatial resolution varied between 1.0 nm (15 kV of accelerating voltage) and 1.4 nm (1 kV).

The breaking force was measured using AGS-X autograph (Shimadzu, Japan) equipped with a 10N high-sensitive detector. The length of the fiber before and after the break was almost equal, indicating the tension of the thread was reversible.

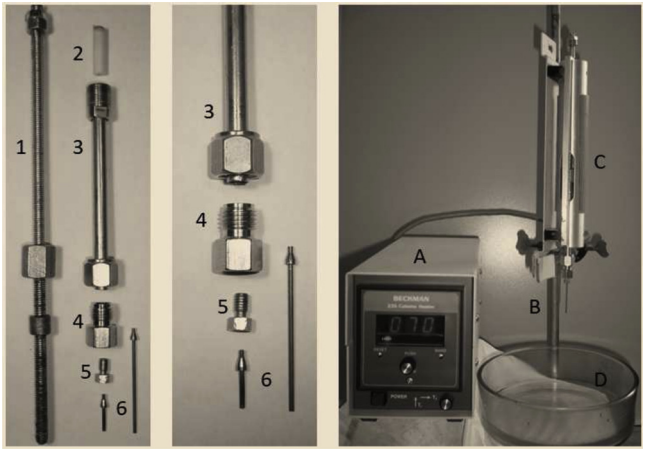

Fig. 1. The laboratory device for fibers production. On the left: *the solution supply system*: 1 – a detail for creating pressure on the piston; 2 – a piston; 3 – a steel tube with collet clamps (a cylinder); 4 – a holder of capillaries, 5 – a clamping nut for capillary mounting, 6 – steel capillaries. On the right: *the assembled device*: A – a heating control unit, B – a tripod, C – a heating element with the cellulose solution supply system, D – a bath filled with cold distilled with water.

The desorption of water from the wet cellulose fibers was analyzed using a gravimetric approach in the temperature range of 28–40 °C (at normal pressure), with an interval of 2 °C, using TC/1-20 SPU thermostat (±0.2°, Smolenskoe SKTB-SPU, Smolensk, Russia). The weight loss was registered in 1 min increments using a DL-120 balance (±0.001 g, AND, Japan).

3. Results

3.1. Structure of cellulose solutions

The structure of cellulose solutions in $[B_{mim}]Cl$ was evaluated microscopically and using the synchrotron radiation diffraction technique. Large anisometric objects (fibers) were found under optical microscope in the solutions of unmercerized hardwood and linter cellulose. In solutions of the unmercerized hardwood cellulose, the fibers' diameter and length were up to 7 μm and 100 μm, respectively (Fig. 2A) that is a bit less than in the initial raw (Nikolsky et al., 2019). However, under the same conditions, the amount of the undissolved fibers in solutions of the mercerized wood cellulose was an order of magnitude lower (data not shown). The same was observed for cotton linter, while there was no difference in solubility of mercerized and unmercerized cotton fibers in $[B_{mim}]Cl$. So, the unmercerized cellulose dissolved in $[B_{mim}]Cl$ worse than the mercerized one, and we used the mercerized cotton linter and hardwood cellulose for films and fibers production.

The dispersion phase presented in the cellulose solutions was analyzed by SEM of the thin film on the glass surface (Fig. 2B). The mercerized wood cellulose films were formed by chaotically distributed fibers of about 20 nm in diameter and 300–400 nm in length. Similar images were obtained for both, mercerized linter cellulose and unmercerized cotton pulp. The width of the fibers composing the films was significantly higher than the nanofibrils' one (2–9 nm), and better corresponded to the native microfibrils' diameter (Fernandes et al., 2011; Hanley et al., 1992; O'Sullivan, 1997; Usov et al., 2015). In the films made of the mercerized wood cellulose, the length of the fibers corresponded to the degree of polymerization of about 600–800, which was two times smaller than the initial value of 1400–1450 found after mercerization. According to the viscosity of the copper-ammonium solution, DP of the mercerized hardwood and cotton linter cellulose after dissolution in $[B_{mim}]Cl$ was approximately the same and equal to 670 ± 150, which is in agreement with the assessment above. The

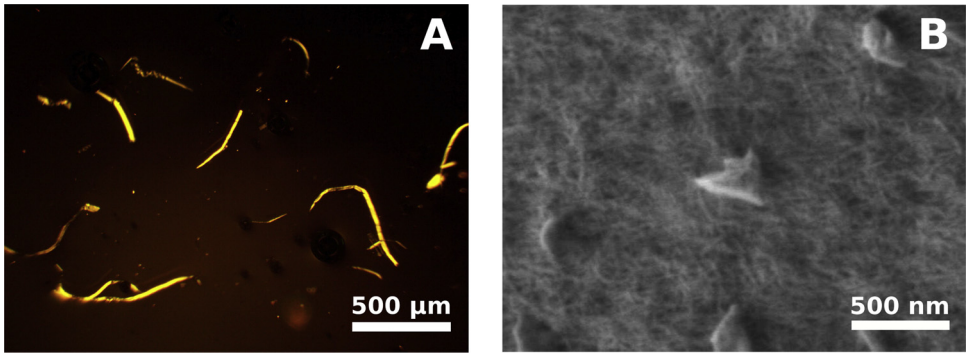

Fig. 2. (A) The optical micrograph of the unmercerized hardwood pulp solution in $[B_{mim}]Cl$ through the crossed polarizers. (B) SEM-image of the film obtained by precipitation of the mercerized hardwood cellulose solution in $[B_{mim}]Cl$ (1%).

degradation of the cotton fiber cellulose was much more prominent, as DP decreased down to 1750 ± 550 after dissolution in $[B_{mim}]Cl$. Probably, such a dramatic, effective decrease appeared due to the preferential dissolution of the low molecular weight fraction of cellulose, while the heavy chains were not dissolved. So, the reduction of the DP in the cotton fiber cellulose should not be treated as a real degradation. Nevertheless, according to the data on the DP of cotton linter and hardwood cellulose, a high-temperature dissolution in $[B_{mim}]Cl$ was accompanied by significant destruction of the macromolecules (Yang et al., 2019).

The homogeneity of the cellulose solutions in $[B_{mim}]Cl$ was examined using a synchrotron radiation diffraction technique. It allowed analyzing the structure of the liquid solution rather than condensed films. The solutions with low concentrations (0.1–2.0%) did not show any noticeable diffraction pattern, whereas the 5% (and more) cellulose solutions demonstrated the expressed diffraction curves (Fig. 3A). The approximation of the diffraction curves by the cylinders' model gives diameters of the fibers of 1.8 and 2.6 nm for wood and cotton (both linter and fibers) cellulose, respectively (Fig. 3B). The obtained values were close to the diameters reported earlier for cellulose nanofibrils of wood and cotton (Fernandes et al., 2011; Usov et al., 2015). So, at low concentrations, the cellulose seems to dissolve in $[B_{mim}]Cl$ right up to macromolecules, whereas at elevated concentrations – only up to nanofibrils.

Note, that the diameters of the fibers revealed in the cellulose solutions (Fig. 3B) and the films (Fig. 2B) were drastically different. In solutions, we detected the dissociated macromolecules or nanofibrils, while much greater structures (similar to microfibrils) were found in the cellulose films. Most probably, these fibrils formed as a result of the secondary agglomeration and twisting together of the macromolecules or nanofibrils in the course of the precipitation (O'Sullivan, 1997).

3.2. Morphology of the fibers

Extrusion of the cellulose solutions to the cold distilled water resulted in the formation of transparent and visually homogeneous fibers (Fig. 4A), and there was no noticeable difference between the fibers made of cotton and wood cellulose. In the case of the smooth movement of the screw, we could have been expected to form the fibers of the homogeneous thickness. However, the diameter of each fiber varied around an average value of about 100 µm (Fig. 4). Most probably, the observed effect appeared as the result of a quasi-periodical regime of the flow of the cellulose solution through the nozzle (Mackarov, 2018; Siginer, 2015). This proposition is confirmed by the decrease of the dispersion of the fibers' diameter with the increase of the dissolution temperature. In particular, for 150 µm cotton fiber the increase of the dissolution temperature from 105° to 130° causes decreasing of the standard deviation for diameter from 20 to 5 µm (at the constant extrusion temperature of 90 °C). Most probably, increasing of the dissolution temperature causes the solution homogenization that causes smoothing of the flow pulsations. The observed fluctuations of the thickness could cause serious degradation in the mechanical properties of the fibers.

The obtained fibers were optically active (Fig. 4B), which is rather a result of their helical structure than the optical activity of the glucose residues themselves (Nikolsky et al., 2019; Zlenko et al., 2019). The rainbow coloring observed in the images implies that the helical pitch of some of the helices in the fibers was close to the wavelength of the visible light (Korolovych et al., 2018), and these helices were oriented parallel to the fiber's axis. The length of these helical structures measured along the continuous colored lines (Fig. 4B) varied between 10 and 100 µm (and more). Most probably, these macroscopic helical structures were formed by agglomerated and twisted nano- and microfibrils detected in the cellulose solutions (Fig. 2, 3). The dimension of the helices found in the fibers denotes that in the course of the

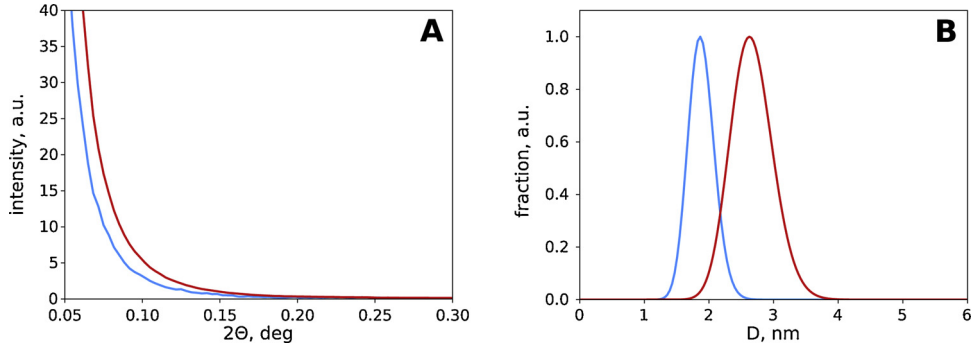

Fig. 3. Synchrotron radiation diffraction curves for the solutions (5%) of the mercerized cotton linter (red line) and mercerized hardwood cellulose (blue line) in $[B_{mim}]Cl$ (A); The distribution of the diameters, calculated according to the diffraction curves approximation by a cylinder model (B).

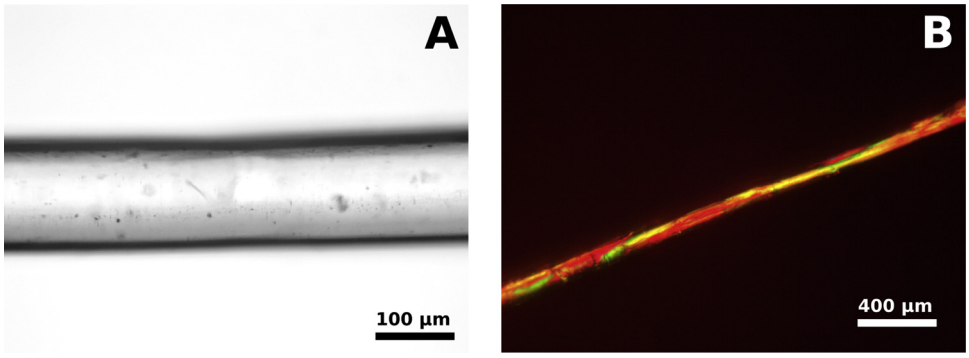

Fig. 4. Optical micrographs of fibers produced by extrusion of mercerized cotton linter cellulose solution (5%) in $[B_{mim}]Cl$ to the cold distilled water: in transmitted light (A) and through crossed polarizers (B).

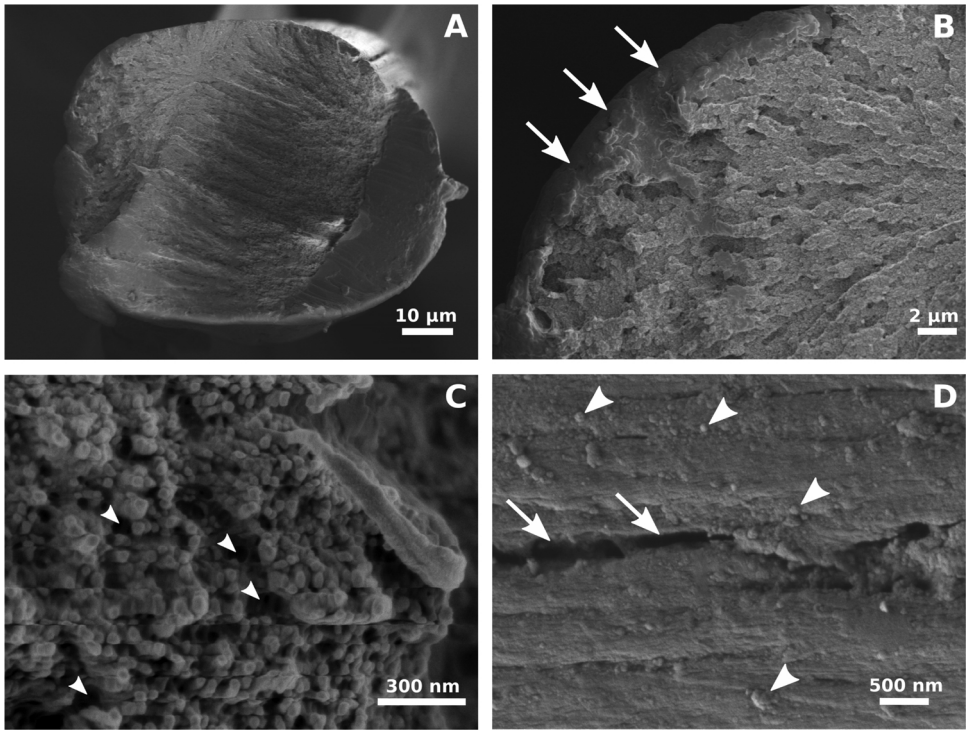

Fig. 5. SEM-images of the fibers produced by the extrusion of the solution (5%) of the mercerized hardwood cellulose in $[B_{mim}]Cl$ into cold distilled water. (A) A general layout of a fiber's cross-section; (B) The enlarged image of the fiber's cross-section. Arrows indicate the shell of the fiber; (C) The fiber's core formed by pseudo-fibrils. Arrowheads mark the interspaces between the pseudo-fibrils; (D) The surface of the fiber. Arrows mark the longitudinal crack, while arrowheads mark the rounded grains.

extrusion process, the cellulose has condensated stronger than in the case of the film formation.

The SEM allowed visualizing of the fiber's internal structure (Fig. 5). The amorphous surface layer of the fibers (a shell) had a thickness in the range of 5–10 µm and was always clearly seen in the fibers' cross sections (Fig. 5B, arrows). The core of the dry fibers was composed of numerous quasi-parallel fibrils (pseudo-fibrils), forming a porous structure (Fig. 5C). On average, the summarized area of cross-sections of all pseudo-fibrils was only 30–40% of the total area of the fiber (Table 1). An average diameter of the pseudo-fibrils was about some dozens of nanometers (Table 1) that is considerably beyond the sizes of typical supramolecular structures in the native cellulose (nano- and microfibrils). The largest average pseudo-fibrils diameter (64 nm) was found in the fibers produced of the cotton linter (5% solution). At the same time, the cross-sections of the wet fibers looked homogeneously and were uniformly filled with a material, and the individual pseudo-fibrils were not revealed (Fig. 7C). Most probably, in the wet fibers, the pseudo-fibrils were swollen (Mantanis, Young, & Rowell, 1994), which could be a reason for the decrease in their strength and increase in elasticity (Wanasekara et al., 2016). The surface of the obtained dry fibers was rough and there were a lot of rounded grains on it (Fig. 5D, arrowheads). Besides that, the surface of the fibers was split by deep

Table 1
The results of the mechanical tests of the fibers prepared by extruding of the cellulose solution in $[B_{mim}]Cl$ into cold distilled water. C.F. – cotton fiber, C.L. – cotton linter, and wood – hardwood cellulose. D – whole fiber diameter, μm; ε – elasticity, %; σ – tensile strength, MPa; E_1, E_2 – Young's modules for steep and smooth parts of the loading curves (Fig. 6), GPa; d – pseudofibrils' diameter, nm; Ω – fraction of the summarized area of the pseudofibrils in the area of the fiber's core cross-section, %. Errors are standard deviations.

Raw	D	ε	σ	E_1	E_2	d	Ω
C.F.	85 ± 26	29 ± 14	260 ± 30	11 ± 7.7	1.1 ± 0.8	35 ± 12	42 ± 14
C.L.	87 ± 22	21 ± 9	247 ± 21	12 ± 5.9	1.9 ± 1.3	36 ± 19	44 ± 12
wood	115 ± 36	12 ± 2.8	242 ± 17	9.3 ± 3.8	2.9 ± 1.7	31 ± 9.1	33 ± 11

longitudinal cracks (Fig. 5D, arrows).

3.3. Mechanical properties of the fibers

The obtained cellulose fibers were strength-tested down to the destruction. Typically, for the dry fibers, the dependence of the load (L) on elongation (ε) had two phases: the initial phase was always steep, while the following part of the curve was more smooth. The Young's modules E_1 and E_2 for these two stages are presented in Table 1 and correspond to the well-known experimental data (Lundahl et al., 2017; Ma et al., 2015; Wanasekara et al., 2016).

A noticeable increase of the strength could be expected at the repeated loading of the fiber that had already been broken once, as the breaking should occur at "the weakest point." However, the tensile strength of the re-tested fibers was statistically indistinguishable from the initial one: the relation of the tensile strengths was 1.1 ± 0.3. At the same time, the elasticity of the re-tested fibers decreased from 29 ± 14% to 2.5 ± 1.1%, for the fibers made of cotton cellulose. This effect was also observed for the fibers of wood cellulose, but to a lesser extent, due to their intrinsically lower elasticity. So, the loading irreversibly modifies the internal structure of the fibers.

The fibers' ends obtained in the strength tests were cylindrical and there was no narrowing zone near the breakpoint (Fig. 7A). At the breakpoint, the shell of the fiber has usually shifted along its axis (Fig. 7A, arrows), so that the core became visible as a set of macroscopic filaments (Fig. 7A, arrowheads).

4. Discussion

4.1. Morphology of the fibers

Narrowing of the fiber at the breakpoint usually appears as the result of the material flowing preceding the break (Argon, 1969). The absence of such a shrinkage (Fig. 7A) implies that the fiber's shell was broken at the lower relative elongation than it was necessary to break the entire fiber. Therefore, the shell is not mechanically strong and does not affect the strength of the fiber. The shell seems to determine only the shape and external diameter of the fibers, whereas the core determines their mechanical properties. This conclusion is supported by the numerous cracks revealed on the surface of the fibers (Fig. 5D, arrows). Under the load, the stress concentrates at the crack's edges, which results in its avalanche-like expansion and breaking of the shell. On the other hand, the tips of the core pseudo-fibrils were clearly narrowed (Fig. 7B), which indicates the flowing of the material of the pseudo-fibrils and supports our conclusion on their mechanical strongness.

There were a lot of isometric grains on the surface of the fibers (Fig. 5D, arrowheads). The smallest ones were found on the surface of the mercerized wood cellulose fibers and had a diameter of about 8 nm. So, they were much greater than platinum particles, which could also be presented on the surface. The volume of these beads was about 250 nm^3. Taking the volume of a single glucose monomer volume equal ~0.3 nm^3, the volume of the macromolecule at PD 600–800 can be estimated as 180–240 nm^3. It allows assuming that the observed grains were compact cellulose macromolecules. The cellulose can be dissolved in $[B_{mim}]Cl$ down to macromolecules, so they can form individual isometric grains. As the grains were found in the fibers' shell only, we can propose that the shell was formed by spherical compact cellulose macromolecules and their aggregates. The packing of the grains was rather loose, as the boundaries between them were well-visible in SEM images (Fig. 5D). Such grained patterns are typical for condensed systems with a large number of nucleations and growth points when the condensed phase areas grow towards each other (Kleman & Lavrentovich, 2003). A piece of additional evidence supporting our assumption on the amorphous structure of the shell can be the absence of any signs of helicity on the fiber's surface, while the whole fibers were optically active and had a helical structure (Fig. 4B).

There were continuous optically active helical envelope-lines on the surface of the fibers (Fig. 4B). The helical pitch of these envelope-lines was about several millimeters. Taking into account the typical size of the nanofibrils (having a few nanometers in thick and up to 500 nm in length), the continuous macroscopic objects (such as the envelope-lines) can form only if nanofibrils associate and twist each other. This suggestion corresponds well to an increase in the diameter of the pseudo-fibrils in the core (tens of nanometers) compared to the nanofibrils observed in the cellulose solutions (Fig. 3). Therefore, we suppose that at the fiber extrusion stage, the nanofibrils associate and form the pseudo-fibrils, which then form the optically active macroscopic helical structures (Fig. 4B). The helicity is a widespread and obligate feature of the supramolecular structures composed of chiral molecules (Nikolsky et al., 2019; Tverdislov, Malyshko, Il'chenko, Zhulyabina, & Yakovenko, 2017). So, we suppose that the pseudo-fibrils also have a helical structure hidden by the amorphous shell of the fiber.

The connectivity of the fibers can be provided by an additional phase acting as a glue and theoretically, water may play such a role. The effective water diffusion coefficient can be defined according to the kinetics of the weight loss by the fiber (data not shown) (Israelachvili, 2011):

$$M(t) = \frac{4M_0}{R}\sqrt{\frac{Dt}{\pi}} \quad (1)$$

where M – evaporated water amount; M_0 – initial weight of the wet fiber; D – diffusion coefficient; and R – fiber radius; t – evaporation time. According to our results, the water diffusion coefficient D inside the fiber was about 4×10^{-11} m^2/s, that is two orders smaller than the water self-diffusion coefficient. Consequently, inside the fibers, water was in the bonded state, and, therefore, it could act as a "molecular glue." This conclusion corresponds to the relatively low strength and

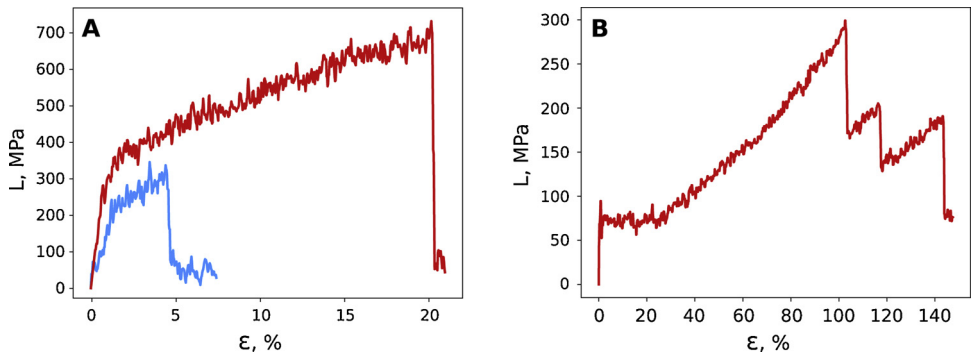

Fig. 6. Loading curves of the single dry fiber (A) and the tow of four wet fibers (B) prepared of the 3% cotton fiber (red) and 5% mercerized hardwood (blue) cellulose solutions in $[B_{mim}]Cl$. The stretching speed was 25 mm/min, the initial fiber length was 50 mm.

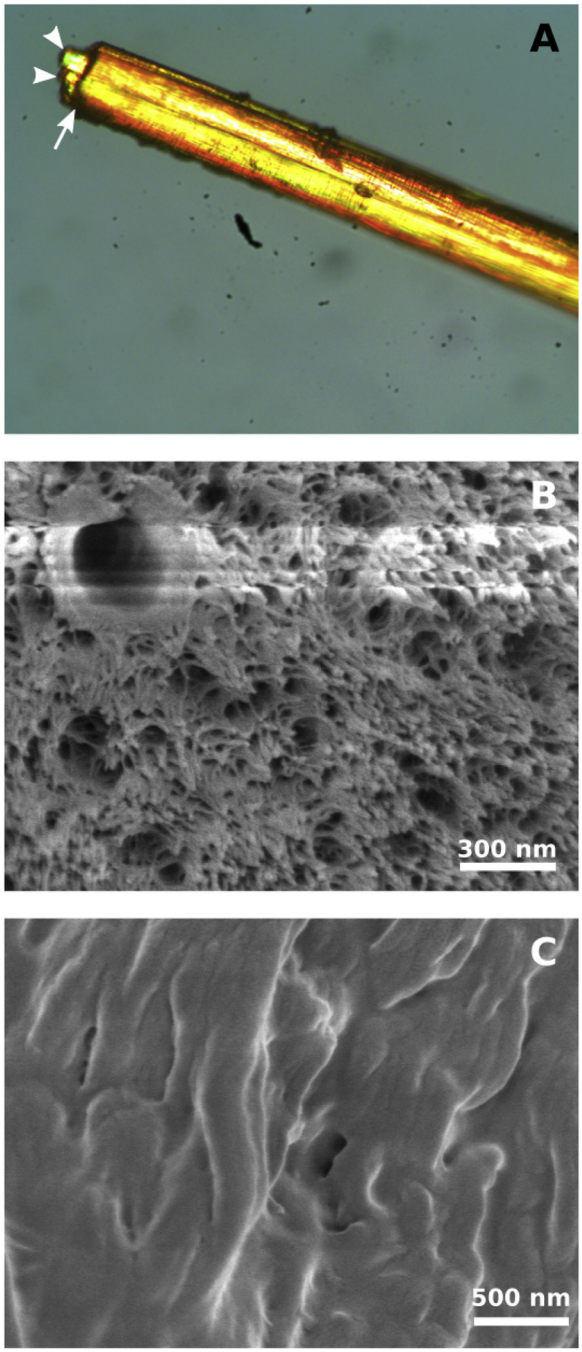

Fig. 7. The images of the ends of the broken fibers prepared by precipitation of the mercerized hardwood cellulose solution (5%) in $[B_{mim}]Cl$. (A) An optical micrograph. The arrow marks the shell, while arrowheads mark the core of the fiber. (B) SEM-image of the dry fiber's end. The pseudo-fibrils were clearly seen, and their ends were narrowed. (C) SEM-image of the wet fiber's end. The pseudo-fibrils were not visualized.

high elasticity of wet fibers (Fig. 6B).

4.2. Orientation of the fibrils

Helicity is the intrinsic property of cellulose (Raabe et al., 2005) that retains even after strong acid or alkaline treatment (Nikolsky et al., 2019). The "reassembling" of the cellulose macromolecules always results in helical structures as in the case of mercerization and cellulose II forming (Dinand et al., 2002; Langan et al., 1999), or the cellulose nitration process leading in helical trinitrate synthesis (Nikolsky et al., 2019). The helicity of the reassembled cellulose could be explained by the sequential processes of the untwisting of cellulose fibers and fibrils followed by their twisting into some new structures (Nikolsky et al., 2019). So, the chaotization of the nanofibrils and/or cellulose chains in the cellulose solutions can significantly affect the properties of the fibers spun of that solutions.

The characteristic time τ of thermally activated orientational relaxation of nanofibrils presented in the cellulose solution (Fig. 2) can be estimated according to the expression derived for the rigid cylinders of a length L and diameter d:

$$\tau = \frac{\pi\eta L^3}{6\mathrm{kT}\ \ln(L/d)} \tag{2}$$

where T – temperature and η – viscosity of the media. The viscosity of 3–5% cellulose solution in $[B_{\mathrm{mim}}]\mathrm{Cl}$ at 70–120 °C lay in the range between 0.1 and 1.0 Pa s for the microcrystalline cellulose having DP of ~180 (Sescousse et al., 2010). According to Piere de Gennes (de Gennes, 1979), the viscosity of the polymer solution has a power-law dependence on the length of the chain, which is confirmed experimentally (Sescousse et al., 2010). The power exponent value as a rule somewhat greater than three (3.2–3.3), while the experimental values could be even greater (Sescousse et al., 2010). In our experiments, the hardwood and cotton linter cellulose had DP of about 700, so the viscosity would be at least 60 times greater, compared to the mentioned above data. So the lower-bound estimate for the viscosity of 5% solution of hardwood or linter cellulose (ν) would be ~10 Pa·s. Therefore, taking into account $T = 373$ K, $L \sim 300$ nm (Fig. 2B) $d \sim 2$ nm (Jarvis, 2003), the relaxation time τ would be at least 5 s. The obtained value is an order of magnitude greater than the time necessary for the solution to pass through the spinneret, so we can neglect the orientational relaxation at this stage.

In the liquid going through the spinneret, the tangential profile of the velocities (v) is:

$$v = \frac{P}{4\eta\Lambda}(R^2 - r^2) \tag{3}$$

where η – viscosity, r – distance to the spinneret axis, P – difference in the pressures at the spinneret ends, R and Λ – radius and length of the spinneret, respectively. Consequently, the pressure difference at the spinneret ends is:

$$P = \frac{4\eta\Lambda v}{R^2} \tag{4}$$

The time required for the orientation of the fibrils in the flow of IL can be assessed based on the tangential profile of the velocities in the spinneret. Since the fibrils are carried by a quite viscous ionic liquid, the velocity of the fibrils' tip (v^*) in relation to its middle point can be estimated as:

$$v^* \sim \frac{\partial v}{\partial r}L \tag{5}$$

So, the characteristic angle rate of the fibril rotation (ω) would be:

$$\omega = \frac{v^*}{L} \sim \frac{\partial v}{\partial r} \sim \frac{\mathrm{Pr}}{\eta\Lambda} \gtrsim \frac{\mathrm{PL}}{\eta\Lambda} \tag{6}$$

This defines the lower-bound estimate for the orientation time (τ^{**}) for the fibrils in the flow:

$$\tau^{**} \sim \frac{1}{\omega} \lesssim \frac{\eta\Lambda}{\mathrm{PL}} \tag{7}$$

The time (t) required for the fibril to pass through the spinneret would be:

$$t = \frac{\Lambda}{v} = \frac{4\eta\Lambda^2}{\mathrm{PR}^2} \tag{8}$$

Comparison of the fibril orientation time (τ^{**}) with the time (t)

required for the fibril to pass the spinneret results in the inequality:

$$\frac{\tau^{**}}{t} \lesssim \frac{R^2}{L\Lambda} \tag{9}$$

So, the fibrils would effectively orient in the spinneret in case if the orientation time is lower than the time the fibril spends on passing through the spinneret. This condition is satisfied if:

$$\Lambda \gg \frac{R^2}{L} \tag{10}$$

At the spinneret radius $R = 125$ μm and the fibril length $L \sim 500$ nm, the spinneret length (Λ) should be much greater than 50 mm. In our experiments, the spinneret was significantly shorter (15 mm). Moreover, the properties of the fibers obtained using a 70 mm spinneret were statistically indistinguishable from the properties of the fibers extruded through 15 mm spinneret. Therefore, both the relative fibrils orientation and formation of the pseudo-fibrils (Fig. 5C) occurred not in the spinneret, but at some other stage of the extrusion process.

The orientation of the nanofibrils could occur as a result of the action of the flow inside the extruder cylinder, rather than in the spinneret. The velocity profile in the spinneret neighborhood with sufficient accuracy has only radial component (V_r) directed to the center of the spinneret:

$$V_r \sim \frac{J}{r^2} \tag{11}$$

where J – is the power of the flow of the liquid into the spinneret. Supposing the fibril to be located on the extruder axis at a distance r from the spinneret ($r \gg d$), and tilted for the angle ϕ to that axis. The fibril would drift towards the spinneret, but "the bottom" end of the fibril would move faster than "the upper" one due to the radial velocity gradient (Eq. 11). This effect would cause the rotating of the nanofibrils at the instantaneous angle rate ω:

$$\omega = \frac{3J}{2r^3}\sin(2\varphi) \tag{12}$$

At the same time, the center of the fibril would drift to the spinneret with a velocity of V_r. Therefore, if the center of fibril shifted on dr, the rotation angle would change on $d\varphi$:

$$d\varphi = \omega \mathrm{d}t = \frac{\omega \mathrm{d}r}{V_r} = \frac{3}{2}\frac{\mathrm{d}r}{r}\sin(2\varphi) \tag{13}$$

Integration of the expression above (Eq. 13) shows that the fibril with an initial tilt of φ_0, and located at a distance r_0 from the spinneret, would have a tilt angle of φ at the closer distance r:

$$\mathrm{tg}\varphi = \mathrm{tg}\varphi_0\left(\frac{r}{r_0}\right)^3 \tag{14}$$

If r and r_0 were close to each other (i.e., the process was running far from the spinneret), then φ would be approximately equal to φ_0. So, the fibrils did not rotate and orient at the large distances from the bottom of the extruder. However, near the spinneret, r could be much smaller than r_0, so tgφ tends to zero. The latter means, the cellulose fibrils become oriented parallel to the spinneret axis and to each other. Thus, according to our estimates, the mutual orientation of the nanofibrils occurs at the spinneret inlet, rather than inside it.

In a real extruder, the flow rate is equal to zero in the boundary layer near its bottom. This would increase both the velocity gradient (Eq. 11) and the effect of orientation of the fibrils. Therefore, the process of fibril's orientation would be even more effective than it follows from the assessments above. On the other hand, slow drifting fibrils coming to the spinneret directly from the boundary layer would orient much worse than the fibrils coming from the extruder's axis. We propose that this effect underlies the forming of the amorphous and mechanically weak shell of the fiber (Figs. 5B and 7A).

4.3. Physical model of the fiber

Let us estimate the fiber's strength based on the conventional understanding of the intermolecular forces providing for the connectedness of the fibers. The interaction energy W of two parallel pseudo-fibrils (Fig. 5C) with a radius R and length L located at a distance h from each other can be estimated as:

$$W = \frac{A\sqrt{R}L}{24\sqrt{h^3}} \tag{15}$$

where A – is a Hamaker constant (Israelachvili, 2011).

At the mutual shifting of the parallel pseudo-fibril along their axis by the value of δL, the length of their engagement zone would reduce by the same value. Respectively, the interaction energy W would decrease by the value of δW:

$$\delta W = \frac{A\sqrt{R}\delta L}{24\sqrt{h^3}} \tag{16}$$

therefore, the restoring force F would be:

$$F = \frac{\delta W}{\delta L} = \frac{A\sqrt{R}}{24\sqrt{h^3}} \tag{17}$$

The Hamaker constant can be approximately estimated as $A \sim 10^{-19}$ J (Israelachvili, 2011); the radius of the pseudo-fibrils R was about 15 nm (Table 1). An average distance between the pseudo-fibrils (h) can be defined based on the density of their packing: in general, pseudo-fibrils occupy about one half of the fiber cross section (Table 1), which results in $h \sim 7$ Å. Using these parameters, we obtained the value of the restoring force (F) of about 10^{-11} N per a pseudo-fibril, and, respectively, about 10^{-4} N per the whole fiber with a diameter of ~100 μm. The obtained value is three orders of magnitude lower than the measured tensile strength of the fibers as well as the stress in the Hooke's region (Fig. 6). For the wet fibers, this value should be yet in order of magnitude lower compared to the dry fibers, due to the decrease of the Hamaker constant (Israelachvili, 2011). Therefore, the interaction of the parallel pseudo-fibrils is too weak and cannot provide for the observed mechanical properties of the fibers in our experiments.

Apart from the above, a friction force (F^*) should act between two parallel pseudo-fibrils. Suggesting the friction force to be a Coulomb one:

$$F^* = \mathrm{k}N \tag{18}$$

where N – is a down-force between the fibers, and k – the friction coefficient, which is generally less than unity (Stiernstedt et al., 2006). The down-force can be calculated as the derivative of the fibril interaction energy (15) with respect to the distance between them:

$$N = -\frac{\partial W}{\partial h} = \frac{A\sqrt{R}L}{16\sqrt{h^5}} \tag{19}$$

If $L \sim 0.3$ μm (Fig. 2B), and the friction coefficient is less than unity, the upper-bound estimate of the friction force would be up to 10^{-8} N per a couple of the fibrils and ~ 0.1 N per the fiber of 100 μm in thick. This value is also significantly smaller than the tensile strength of the obtained fibers. Consequently, the friction force on its own also cannot provide for the observed strength of the cellulose fibers. We suppose that the fibers may become stronger due to the pseudo-fibrils twisting that is usual for condensed chiral phases, in general (Stovbun, Skoblin, & Zlenko, 2018) and cellulose, in particular (Nikolsky et al., 2019; Raabe et al., 2005). The friction force between the twisted pseudo-fibrils (F) increases exponentially with the number of turns (α) according to the Capstan equation (Nikolsky et al., 2019):

$$F = F_0 \exp(2\pi\alpha k) \tag{20}$$

where F_0 – the friction force between two parallel fibrils (Eq. 17). So, even a few mutual twists of the pseudo-fibrils seem to be sufficient to

provide for the experimentally observed strength of the fibers.

The hypothesis on the role of the friction in the strength of the fibers is supported by the shape of the stress-strain curves, which always consisted of two stages: steep and smooth (Fig. 6, Table 1). Similar curves were reported for lots of other fibers (Lundahl et al., 2017; Ma et al., 2015; Wanasekara et al., 2016) that support the generality of the phenomenon. The first (steep) stage in the stress–strain curves can be related to the Hooke's deformation of the fiber as a whole, while the second one (smooth) – to the slipping the twisted pseudo-fibrils in respect to each other. A similar hypothesis was suggested earlier, but the helical structure of the fibers was not taken into account (Wanasekara et al., 2016). This hypothesis also explains the properties of the wet fibers. Indeed, the increase in water amount in the fibers should cause the growth of the amount of free water, which acts as a molecular “lubricant”, resulting both in the decrease of the friction coefficient between the fibrils and the strength of the whole fiber. Moreover, according to this hypothesis, the process of stretching of the wet fibers should be smooth, free of the saltatory variations in the number of mutual twists, which explains the observed increase of their elasticity (Fig. 6B).

The proposed hypothesis explains the similarity in the mechanical properties of the artificial fibers made of the cellulose of different origin and DP. According to our hypothesis, the strength of the fibers is defined by the interaction between the pseudo-fibrils, rather than by the properties of the pseudo-fibrils themselves. Indeed, in the course of stretching, the number of pseudo-fibrils in the fiber's cross-section decreases, as they slip in respect to each other. Therefore, the fiber would break when the number of pseudo-fibrils fell to some critical threshold. In this case, the force required for fiber break, first of all, would depend on the fiber elongation, rather than on the strength of the individual pseudo-fibril.

Optimization of the production technique theoretically allows reducing the thickness of the amorphous shell and increasing the density of the packing of the pseudo-fibrils in the core. In our experiments, some of the fibers had the tensile strength up to 0.9 GPa that is three times greater than the average value of ~250 MPa. Accordingly, we would like to provide an estimate on the tensile strength for a hypothetical fiber formed by densely packed pseudo-fibrils and devoid of the shell. The fibers, made of the cotton cellulose had an average diameter of 85 μm and a shell thickness up to 10 μm, which is about 40% of the area of the fiber's cross-section. The summarized area of the pseudo-fibrils in the core of these fibers was approximately 40% of the area of the core cross-section. Consequently, the effective tensile strength of the cotton pseudo-fibrils can be evaluated as ~1.1 GPa. In the case of the fibers of wood cellulose, the share of the area of the pseudo-fibrils area was smaller, but the diameter of the fibers was greater (Table 1), so, the tensile strength of the ideal fiber appeared to be approximately the same (1.1 GPa).

5. Conclusion

The obtained fibers demonstrated middle-of-the-road values of the tensile strength (Table 1), which were smaller than for some of the described earlier samples (Gindl et al., 2008; Hummel et al., 2006; Mittal et al., 2018; Northolt et al., 2001; Perepelkin, 2007; Röder et al., 2009). However, the fibers produced using the cotton cellulose were characterized by a very high elasticity (up to 40%), which is an outstanding feature (Gindl et al., 2008; Röder et al., 2009).

Let us consider the fiber as a component of the ballistic fabric designed for retarding a projectile. Smith's formula (Smith, McCrackin, & Schiefer, 1958) defines the relations between the strain in the fiber (σ), its properties, and the velocity (v) of the projectile (for a transverse impact):

$$\sigma = \sqrt[3]{\frac{E\rho^2 v^4}{4}} \quad (21)$$

where E – is Young's modulus and ρ – the fiber density (~ 1.5 g/cm^3). Considering the second (elastic) stage of the tension curve, Young's modulus for the cotton cellulose-based fibers can be assumed to be about 1 GPa (Table 1). The fabrics made of such fibers allow retarding the projectile having a velocity up to 450 m/s.

There was a negative correlation between Young's modulus at the second (elastic) stage of the loading curve and the overall strength of the fibers. For the best samples, Young's modulus at the second elastic stage was less than 0.5 GPa, whereas the tensile strength reached up to 600–900 MPa. The fabrics woven of such fibers would be ably retarding the projectile having a velocity up to 900–1200 m/s. It should be emphasized that using weak (280 MPa) but very elastic (20–30%) fibers would significantly extend the time of the retarding and, consequently, amortize the strike. Under otherwise identical conditions, the fold increase of the strike time would lead to a proportional decrease in the peak loads on a secured object. So, the protective shell composed of the elastic fibers would not only retard the projectile but also appreciably weakens the strike, in contrast to a protection layer formed by stronger but less elastic fibers.

References

Argon, A. S. (1969). *Physics of strength and plasticity*. Massachusetts, USA: MIT Press.

Asaadi, S., Hummel, M., Hellsten, S., Härkäsalmi, T., Ma, Y., Michud, A., & Sixta, H. (2016). Renewable high-performance fibers from the chemical recycling of cotton waste utilizing an ionic liquid. *ChemSusChem, 9*, 1–10.

Boerstoel, H., Maatman, H., Westerink, J., & Koenders, B. (2001). Liquid crystalline solutions of cellulose in phosphoric acid. *Polymer, 42*, 7371–7379.

Cross, C., & Bevan, E. (1892). Improvements in dissolving cellulose and allied compounds. British Patent Application, 8, 700.

Dawsey, T., & McCormic, C. (1990). The lithium chloride/dimethylacetamide solvent for cellulose: A literature review. *Reviews on Macromolecular Chemistry and Physics, 30*, 405–440.

Dinand, E., Vignon, M., Chanzy, H., & Heux, L. (2002). Mercerization of primary wall cellulose and its implication for the conversion of cellulose I → cellulose II. *Cellulose, 9*, 7–18.

Dupont, J., Consorti, C. S., Suarez, P. A., & de Souza, R. F. (2003). Preparation of 1-butyl-3-metyl imidazolium-based room temperature ionic liquids. *Organic Syntheses, 79*, 236–243.

Endo, T., Hosomi, S., Fujii, S., Ninomiya, K., & Takahashi, K. (2016). Anion bridging-induced structural transformation of cellulose dissolved in ionic liquid. *The Journal of Physical Chemistry Letters, 7*, 5156–5161.

Fendt, S., Padmanabhan, S., Blanch, H. W., & Prausnitz, J. M. (2011). Viscosities of acetate or chloride-based ionic liquids and some of their mixtures with water or other common solvents. *Journal of Chemical and Engineering Data, 56*, 31–34.

Fernandes, A., Thomas, L., Altaner, C., Callow, P., Forsyth, V., Apperley, D., Kennedy, C., & Jarvis, M. (2011). Nanostructure of cellulose microfibrils in spruce wood. *Proceedings of the National Academy of Sciences of the United States of America, 108*, E1195–E1203.

Fukaya, Y., Sugimoto, A., & Ohno, H. (2006). Superior solubility of polysaccharides in low viscosity, polar, and halogen-free 1,3-dialkylimidazolium formates. *Biomacromolecules, 7*, 3295–3297.

de Gennes, P.-G. (1979). *Scaling concepts in polymer physics. Chapter VIII. Entanglement effects*. London, UK: Cornell University Press219–244.

Gindl, W., Reifferscheid, M., Adusumalli, R., Weber, H., Röder, T., Sixta, H., & Schöberl, T. (2008). Anisotropy of the modulus of elasticity in regenerated cellulose fibres related to molecular orientation. *Polymer, 49*, 792–799.

Graenacher, C. (1934). Cellulose solution. US Patent 1934176 A.

Graenacher, C., & Sallmann, R. (1939). Cellulose solution and process of making same. US Patent 2179181 A.

Hanley, S. J., Giasson, J., Revol, J.-F., & Gray, D. G. (1992). Atomic force microscopy of cellulose microfibrils: Comparison with transmission electron microscopy. *Polymer, 33*, 4639–4642.

Hanley, S. J., Revol, J.-F., Godbout, L., & Gray, D. G. (1997). Atomic force microscopy and transmission electron microscopy of cellulose from *Micrasterias denticulate*: Evidence for a chiral helical microfibril twist. *Cellulose, 4*, 209–220.

Heinze, T., & Koschella, A. (2005). Solvents applied in the field of cellulose chemistry – A mini review. *Polímeros: Ciência e Tecnologia, 15*, 84–90.

Hina, S., Zhang, Y., & Wang, H. (2015). Role of ionic liquids in dissolution and regeneration of cellulose. *Reviews on Advanced Materials Science, 40*, 215–226.

Hishikawa, Y., Togawa, E., & Kondo, T. (2010). Molecular orientation in the nematic ordered cellulose film using polarized FTIR accompanied with a vapor-phase deuteration method. *Cellulose, 17*, 539–545.

Hult, E., Larsson, P., & Iversen, T. (2001). Cellulose fibril aggregation – An inherent property of kraft pulps. *Polymer, 42*, 3309–3314.

Hummel, M., Michud, A., Tanttu, M., Asaadi, S., Ma, Y., Hauru, L. K., Parviainen, A., King, A. W., Kilpelaine, I., & Sixta, H. (2006). Ionic liquids for the production of man-made cellulosic fibers: Opportunities and challenges. In O. J. Rojas (Ed.). *Cellulose chemistry and properties: Fibers, nanocelluloses and advanced materials* (pp. 133–168).

Switzerland: Springer International Publishing.
Israelachvili, N. (2011). *Intermolecular and surface forces.* London, UK: Elsevier.
Jarvis, M. (2003). Cellulose stacks up. *Nature, 426*, 611–612.
Kamide, K., Okajima, K., & Kowsaka, K. (1992). Dissolution of natural cellulose into aqueous alkali solution: Role of supramolecular structure of cellulose. *Polymer Journal, 24*, 71–86.
Kim, D. B., Pak, J. J., Jo, S. M., & Lee, W. S. (2005). Dry jet-wet spinning of cellulose/N-methylmorpholine N-oxide hydrate solutions and physical properties of lyocell fibers. *Textile Research, 75*, 331–341.
Kleman, M., & Lavrentovich, O. D. (2003). *SoftMatter physics: An introduction.* Switzerland: Springer International Publishing.
Korolovych, V. F., Cherpak, V., Nepal, D., Ng, A., Shaikh, N. R., Grant, A., Xiong, R., Bunning, T. J., & Tsukruk, V. V. (2018). Cellulose nanocrystals with different morphologies and chiral properties. *Polymer, 145*, 334–347.
Kostag, M., Jedvert, K., Achtel, C., Heinze, T., & Seoud, O. A. E. (2018). Recent advances in solvents for the dissolution, shaping and derivatization of cellulose: Quaternary ammonium electrolytes and their solutions in water and molecular solvents. *Molecules, 23*, E511.
Langan, P., Nishiyama, Y., & Chanzy, H. (1999). A revised structure and hydrogen-bonding system in cellulose II from a neutron fiber diffraction analysis. *Journal of the American Chemical Society, 121*, 9940–9946.
Lundahl, M. J., Klar, V., Wang, L., Ago, M., & Rojas, O. J. (2017). Spinning of cellulose nanofibrils into filaments: A review. *Industrial & Engineering Chemistry Research, 56*, 8–19.
Ma, Y., Asaadi, S., Johansson, L.-S., Ahvenainen, P., Reza, M., Alekhina, M., Rautkari, L., Michud, A., Hauru, L., Hummel, M., & Sixta, H. (2015). High-strength composite fibers from cellulose-lignin blends regenerated from ionic liquid solution. *ChemSusChem, 8*, 4030–4039.
Mackarov, I. A. (2018). On some key problems of modern polymer rheology. *Journal of Polymer Science Engineering*.
Mantanis, G., Young, R., & Rowell, R. (1994). Swelling of wood. Part 1. Swelling in water. *Wood Science and Technology, 28*, 119–134.
Meyer, K. H., & Misch, L. (1937). Positions des atomes dans le nouveau modele spatiall de la cellulose. *Helvetica, 20*, 232–244.
Michud, A., Hummel, M., & Sixta, H. (2016). Influence of process parameters on the structure formation of man-made cellulosic fibers from ionic liquid solution. *Journal of Applied Polymer Science, 133*, E43718.
Mittal, N., Ansari, F., V, K. G., Brouzet, C., Chen, P., Larsson, P. T., Roth, S. V., Lundell, F., Wågberg, L., Kotov, N. A., & Söderberg, L. D. (2018). Multiscale control of nanocellulose assembly: Transferring remarkable nanoscale fibril mechanics to macroscale fibers. *ACS Nano, 12*, 6378–6388.
Morgenstern, B., & Kammer, H.-W. (1999). On the particulate structure of cellulose solutions. *Polymer, 40*, 1299–1304.
Newman, R. (1999). Estimation of the lateral dimensions of cellulose crystallites using ^{13}C NMR signal strengths. *Solid State Nuclear Magnetic Resonance, 15*, 21–29.
Nikolsky, S. N., Zlenko, D. V., Melnikov, V. P., & Stovbun, S. V. (2019). The fibrils untwisting limits the rate of cellulose nitration process. *Carbohydrate Polymers, 204*, 232–237.
Nishino, T., Takano, K., & Nakamae, K. (1995). Elastic modulus of the crystalline regions of cellulose polymorphs. *Journal of Polymer Science, 33*, 1647–1651.
Northolt, M., Boerstoel, H., Maatman, H., Huisman, R., Veurink, J., & Elzerman, H. (2001). The structure and properties of cellulose fibres spun from an anisotropic phosphoric acid solution. *Polymer, 42*, 8249–8264.
Oksman, K., Aitomäki, Y., Mathew, A. P., Siqueira, G., Zhou, Q., Butylina, S., Tanpichai, S., Zhou, X., & Hooshmand, S. (2016). Review of the recent developments in cellulose nanocomposite processing. *Composites, 83*, 2–18.
O'Sullivan, A. C. (1997). Cellulose: The structure slowly unravels. *Cellulose, 4*, 173–207.
Oudiani, A. E., Chaabouni, Y., Msahli, S., & Sakli, F. (2011). Crystal transition from cellulose I to cellulose II in NaOH treated Agave americana l. Fibre. *Carbohydrate Polymer, 86*, 1221–1229.
Perepelkin, K. (2007). Lyocell fibres based on direct dissolution of cellulose in N-methylmorpholine N-oxide: Development and prospects. *Fibre Chemistry, 39*, 163–172.
Raabe, D., Sachs, C., & Romano, P. (2005). The crustacean exoskeleton as an example of a structurally and mechanically graded biological nanocomposite material. *Acta Materialia, 53*, 4281–4292.
Rabideau, B. D., & Ismail, A. E. (2015). Effect of water content in N-methylmorpholine N-oxide/cellulose solutions on thermodynamics, structure, and hydrogen bonding. *Journal of Physical Chemistry B, 119*, 15014–15022.
Richter, G. (1929). Process for the production of high-alpha cellulose fiber for the manufacture of cellulose derivatives. US Patent 1741540 A.
Röder, T., Moosbauer, J., Kliba1, G., Schlader, S., Zuckerstätter, G., & Sixta, H. (2009). Comparative characterization of man-made regenerated cellulose fibres. *Lenzinger Berichte, 87*, 98–105.
Sealey, J.E., Persinger, W.H., Luo, M., Roscelli, V.A., & Neogi, A.N. (2002). Process for making Lyocell fibers from alkaline pulp having low average degree of polymerization values. US Patent 6491788 B2.
Sescousse, R., Le, K. A., Ries, M. E., & Budtova, T. (2010). Viscosity of cellulose-imidazolium-based ionic liquid solutions. *Journal of Physical Chemistry, 114*, 7222–7228.
Siginer, D. A. (2015). *Quasi-periodic flows of viscoelastic fluids in straight tubes. Developments in the flow of complex fluids in tubes*. Switzerland: Springer International Publishing65–78 chapter 5.
Smith, J. C., McCrackin, F. L., & Schiefer, H. F. (1958). Stress–strain relationships in yarns subjected to rapid impact loading: 5. Wave propagation in long textile yarns impacted transversely. *Journal of Research of the National Institute of Standards, 60*, 517–534.
Song, H., Niu, Y., Wang, Z., & Zhang, J. (2011). Liquid crystalline phase and gel–sol transitions for concentrated microcrystalline cellulose (MCC)/1-ethyl-3-methylimidazolium acetate (EMIMAC) solutions. *Biomacromolecules, 12*, 1087–1096.
Stiernstedt, J., Nordgren, N., Wagberg, L., Brumer, H., Gray, D., & Rutland, M. (2006). Friction and forces between cellulose model surfaces: A comparison. *Journal of Colloid and Interface Science, 303*, 117–123.
Stovbun, S. V., Skoblin, A. A., & Zlenko, D. V. (2018). Self assembly and gelation in solutions of chiral N-trifluoroacetylated α-aminoalcohols. *Chemical Physics, 508*, 34–44.
Swatloski, R. P., Spear, S. K., Holbrey, J. D., & Rogers, R. D. (2002). Dissolution of cellulose with ionic liquids. *Journal of the American Chemical Society, 124*, 4974–4975.
Tashiro, K., & Kobayashi, M. (1990). Theoretical evaluation of three-dimensional elastic constants of native and regenerated celluloses: Role of hydrogen bonds. *Polymer, 32*, 1516–1526.
Tverdislov, V., Malyshko, E., Il'chenko, S., Zhulyabina, O., & Yakovenko, L. (2017). A periodic system of chiral structures in molecular biology. *Biophysics, 62*, 331–341.
Usov, I., Nyström1, G., Adamcik, J., Handschin, S., Schütz, C., Fall, A., Bergström, L., & Mezzenga, R. (2015). Understanding nanocellulose chirality and structure-properties relationship at the single fibril level. *Nature Communication, 6*, E7564.
Vanhoorne, M., van der Berge, L., Devreese, A., Tijtgat, E., van Pouke, L., & van Peteghem, C. (1991). Survey of chemical exposures in a viscose rayon plant. *Annals of Occupational Hygiene, 35*, 619–631.
Wanasekara, N. D., Michud, A., Zhu, C., Rahatekar, S., Sixta, H., & Eichhorn, S. J. (2016). Deformation mechanisms in ionic liquid spun cellulose fibers. *Polymer, 99*, 222–230.
Whorlow, R. (1980). *Rheological techniques.* Chichester, UK: Ellis Horwood.
Yang, J., Lu, X., Yao, X., Li, Y., Yang, Y., Zhou, Q., & Zhang, S. (2019). Inhibiting degradation of cellulose dissolved in ionic liquids via amino acids. *Green Chemistry, 21*, 2777.
Zhang, Y. P., Cui, J., Lynd, L. R., & Kuang, L. R. (2006). A transition from cellulose swelling to cellulose dissolution by o-phosphoric acid: Evidence from enzymatic hydrolysis and supramolecular structure. *Biomacromolecules, 7*, 644–648.
Zhao, Y., & Li, J. (2014). Excellent chemical and material cellulose from tunicates: Diversity in cellulose production yield and chemical and morphological structures from different tunicate species. *Cellulose, 21*, 3427–3441.
Zlenko, D. V., Nikolsky, S. N., Vedenkin, A. S., Politenkova, G. G., Skoblin, A. A., Melnikov, V. P., Mikhaleva, M. G., & Stovbun, S. V. (2019). Twisting of fibers balancing the gel–sol transition in cellulose aqueous suspensions. *Polymers, 11*, 873.